RSC Advances

PAPER

View Article Online
View Journal | View Issue

Cite this: *RSC Adv.*, 2019, **9**, 23261

Role of polysilicon in poly-Si/SiO_x passivating contacts for high-efficiency silicon solar cells

HyunJung Park, *[a] Soohyun Bae,[a] Se Jin Park,[a] Ji Yeon Hyun,[a] Chang Hyun Lee,[a] Dongjin Choi,[a] Dongkyun Kang,[a] Hyebin Han,[a] Yoonmook Kang,†[b] Hae-Seok Lee†[b] and Donghwan Kim†[ab]

Received 12th May 2019
Accepted 22nd July 2019

DOI: 10.1039/c9ra03560e

rsc.li/rsc-advances

In this study, we focused on understanding the roles of a polysilicon (poly-Si) layer in poly-Si/SiO_x/c-Si passivating contacts. Passivating contact formation conditions were varied by changing the doping method, annealing temperature and time, polysilicon layer thickness, and polysilicon doping concentration. Our observations indicated that the roles of polysilicon are contact, in-diffusion barrier action, field effect, gettering, and light absorption. Based on the observations, a iV_{OC} of 741 mV was obtained. Finally, to increase J_{SC} with high V_{OC}, the polysilicon was etched after hydrogenation to reduce light absorption with high passivation quality. iV_{OC} was not affected by etching; moreover, by etching the polysilicon from 300 nm to 60 nm, the cell efficiency increased from 20.48% to 20.59% with increasing J_{SC}, constant V_{OC}, and fill factor.

1 Introduction

As the theoretical efficiency limit for silicon solar cells is approaching,[1] various solar cell structures and fabrication methods are being studied. In a solar cell, carriers are generated by incident light and collected on external electrodes. In this process, electrons and holes are separately collected on each electrode by carrier selectivity.[2] For a conventional structure of silicon solar cell with aluminum back surface field (Al-BSF), recombination loss at the metal–semiconductor junction is the major cause of efficiency loss owing to the high interface defect density at the metal/silicon interface.[3–5] To reduce the recombination loss, passivating contacts (also referred to as carrier-selective contacts) have been introduced for high-quality passivation with low contact resistance.[2,5–14] The passivating contact cells differ from conventional cells in the following ways: (1) the recombination occurring at the metal–semiconductor junction is reduced by a passivation layer between the crystalline silicon and metal contact, and (2) the majority carriers can move to the metal contact, while the minority carriers cannot be moved from crystalline silicon to the metal contact owing to carrier selectivity.

The major two passivating contacts use intrinsic amorphous silicon (a-Si) or silicon oxide (SiO_x) as a thin passivation layer. Passivating contacts based on a-Si are referred to as heterojunction or HIT.[15–18] The SiO_x-based passivating contacts consist of SiO_x and polycrystalline silicon (poly-Si) in a stack structure, and the cells using poly-Si/SiO_x passivating contacts are referred to as tunnel oxide passivated contact (TOPCon),[8,19–22] semi-insulating polycrystalline silicon (SIPOS),[23,24] polycrystalline silicon on oxide (POLO),[25,26] or poly-Si passivating contact.[27–30] Additionally, it should be noted that EPFL recently published a study on SiO_x-based passivating contact using silicon-rich silicon carbide instead of poly-Si.[31] In HIT cells, the highest recorded efficiency for an interdigitated back contact (IBC) structure was 26.7% (ref. 16 and 17) and that for a front and rear contact structure was 24.7%.[18] However, heterojunction solar cells have process temperature limits.[32–36] Therefore, another passivating contact structure with SiO_x/poly-Si, instead of amorphous silicon, has attracted the interest of researchers. In poly-Si passivating contact cells, the highest efficiency of 26.1% and 25.8% for IBC[25] and front and rear contact structures[17,37] were reported, respectively. This efficiency is remarkable because it is the highest efficiency using the front and rear contact.

With respect to poly-Si passivating contact, many researchers have focused on understanding the characteristics of silicon oxide.[9,38–41] In this research, we attempted to focus on poly-Si to understand the relationship between poly-Si and the properties of passivating contact solar cells including electrical and passivation properties. Thus, in this study, we varied the doping method, annealing temperature and time, poly-Si thickness, and doping concentration. For the characterization, we measured the implied open circuit voltage (iV_{OC}), doping concentration profile, and the thickness and crystallinity of poly-Si using quasi-steady-state photoconductance (QSSPC),[42]

[a]*Department of Materials Science and Engineering, Korea University, Seoul 02841, Republic of Korea. E-mail: jung1029@korea.ac.kr; Tel: +02 3290 3713*

[b]*KU-KIST Green School Graduate School of Energy and Environment, Korea University, Seoul 02841, Republic of Korea*

† These authors contributed equally to this work.

secondary ion mass spectroscopy (SIMS), transmission electron microscopy (TEM), and atom probe tomography (ATP), respectively.

2 Experimental procedure

N-type crystalline silicon wafers grown using the Czochralski method were used. The thickness and resistivity of the wafer were 180 μm and 4.5 Ω cm, respectively. After saw-damage etching using KOH, a silicon oxide layer with a thickness of 1.2 nm was grown on the wafer surface *via* wet chemical oxidation using H_2O_2.[43] Subsequently, two types of poly-Si layers: intrinsic poly-Si and *in situ* P-doped poly-Si, were deposited on the silicon oxide surface using low pressure chemical vapor deposition (LPCVD) equipment at 600 °C. The thickness of the intrinsic poly-Si was varied from 50 to 300 nm and $POCl_3$ diffusion was conducted to dope the intrinsic poly-Si. In the pre-deposition step, a $POCl_3 : O_2$ gas mixture with varied ratio from 200 : 800 to 800 : 200 was used to control the poly-Si doping concentration. The deposition temperature and time were fixed at 740 °C and 20 min, respectively. After pre-deposition, the samples were annealed at temperatures between 800 and 950 °C from 10 to 60 min in a N_2 atmosphere. For *in situ* P-doped poly-Si, the samples were annealed in the same furnace that was used to anneal $POCl_3$-diffused poly-Si in the N_2 atmosphere after the deposition of the *in situ* P-doped poly-Si. The annealing temperature and time were changed from 800 to 950 °C and 10 to 60 min, respectively. After annealing, both $POCl_3$-diffused poly-Si and *in situ* P-doped poly-Si were dipped in diluted HF acid to etch PSG and native SiO_x on poly-Si. Subsequently, the samples were subjected to hydrogenation to further improve the passivation quality by depositing the stacked layers of SiN_x and Al_2O_3 with subsequent annealing at 600 °C for 15 min in a N_2 atmosphere. Plasma-enhanced chemical vapor deposition (PECVD) and atomic layer deposition (ALD) were used to deposit SiN_x and Al_2O_3, and rapid thermal process (RTP) was used to anneal them. The stacked layers of SiN_x and Al_2O_3 were removed by dipping in diluted HF. For subsequent experiments on etching poly-Si, an acidic mixture composed of $HNO_3 : H_2O : HF = 300 : 100 : 10$ by volume was used. The passivation quality of the poly-Si contact was analyzed by iV_{OC}, measured using the QSSPC. The doping concentration profile was measured using SIMS measurement. TEM measurement was used to confirm the thickness and crystallinity of the poly-Si. Moreover, after preparing the abovementioned sandwich-structured samples to measure the QSSPC, we fabricated the passivating contact solar cell. The schematics of detailed sample structure and cell structure are presented in Fig. 1.

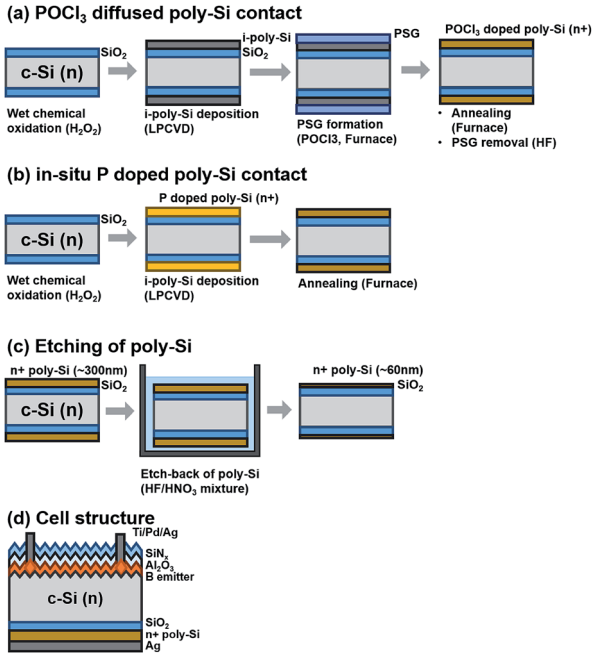

Fig. 1 Schematic of sample structure for (a) $POCl_3$-diffused poly-Si contact, (b) *in situ* P-doped poly-Si contact, (c) etched poly-Si contact, and (d) the final cell structure.

3 Results

3.1 Controlling passivation quality

3.1.1 Comparison of doping methods and poly-Si thickness. First, we compared two doping methods to form n+ poly-Si, namely, *ex situ* doping by depositing intrinsic poly-Si through LPCVD and phosphorus doping through $POCl_3$ diffusion, and *in situ* doping by directly depositing the phosphorus doped poly-Si using LPCVD. As the annealing temperature and time increased, the passivation quality of the poly-Si contacts changed, as shown in Fig. 2(a). Increasing the annealing temperature improved the passivation quality, and increasing the annealing time led to the commencement of deterioration of iV_{OC} for both *ex situ*- and *in situ*-doped poly-Si contacts. Moreover, iV_{OC} of the *in situ* P poly-Si was higher than that of the $POCl_3$-diffused poly-Si, and the decrease in the rate of iV_{OC} of *in situ* P poly-Si was lower than that of $POCl_3$-diffused poly-Si.

Thus, a different iV_{OC} behavior between *in situ* P poly-Si and $POCl_3$-diffused poly-Si in the degradation rate of iV_{OC} could be due to the PSG layer. The doping concentration of PSG layer is approximately 1×10^{21} cm^{-3}, which generates three times higher flux because the doping concentration difference between $POCl_3$-diffused poly-Si and *in situ* P doped poly-Si is three times greater. Owing to this high flux, the dopant atoms diffuse from PSG to poly-Si. This accelerates the deterioration of iV_{OC} as the diffusion of P from poly-Si to c-Si increases, as shown in Fig. 2(d). Consequently, an important role of poly-Si is that of an in-diffusion barrier. It should be noted that the *in situ* doping method is more suitable owing to a lower extent of in-diffusion.

Additionally, we grew a PSG layer on *in situ* poly-Si to investigate the effect of a PSG formation step on the characteristics of the poly-Si contact. After growing the PSG layer, it was removed and annealed at 950 °C for 20 min in N_2. Consequently, the addition of the PSG growth step decreased the iV_{OC} by 15 mV. This result indicates that the PSG growth step affects passivation quality. A further in-depth study will be required to understand the cause of iV_{OC} due to the addition of the PSG

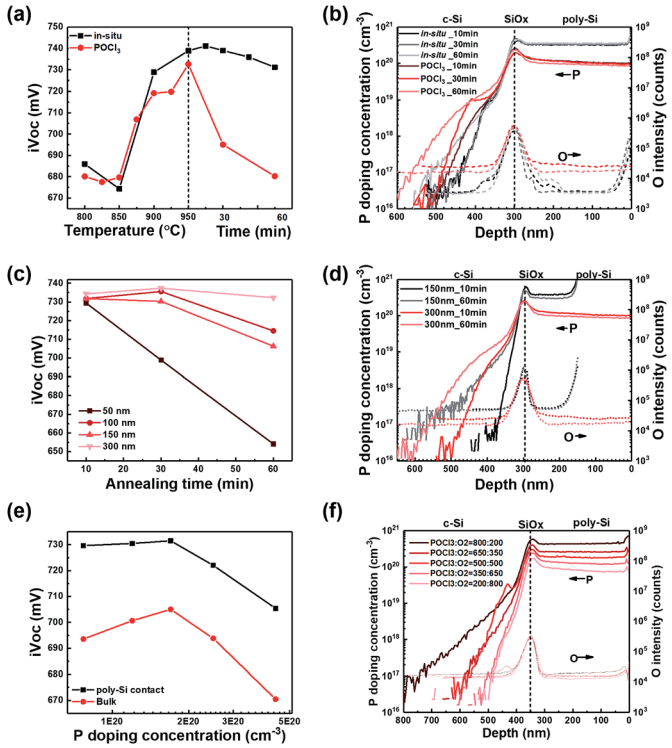

Fig. 2 iV_{OC} of poly-Si passivating contacts as a function of (a) annealing temperature, time required for different doping methods, and (c) annealing time for different thicknesses. (e) P doping concentration at poly-Si. (b, d, f) P doping concentration profile (solid line) and oxygen intensity profile (dotted line) of (a, c, e), respectively.

formation step as well as the effect of the PSG growth step on the tunnel oxide or poly-Si layer.

3.1.2 Comparison of thicknesses of poly-Si. Second, we changed the thickness of poly-Si from 50 to 300 nm by depositing different thicknesses of intrinsic poly-Si with subsequent doping process using $POCl_3$ diffusion with annealing at 950 °C for 10 min. From the first experimental result, a change in the thickness of poly-Si was expected to affect the rate of decrease in iV_{OC} because the in-diffusion would be higher for a thinner poly-Si. To verify this, we deposited intrinsic poly-Si with different thicknesses varying from 50 to 300 nm. The decrease in iV_{OC} was accelerated with the decreasing thickness of poly-Si. This indicates that poly-Si should act as an in-diffusion barrier and should be sufficiently thick to prevent in-diffusion according to the annealing temperature and time.

3.1.3 Comparison of doping concentrations. Third, the doping concentration at poly-Si was controlled by varying the mixture ratio of the source gas in the pre-deposition step. Thus, the poly-Si doping concentration was changed from 8×10^{19} cm^{-3} to 4.5×10^{20} cm^{-3} as the $POCl_3$: O_2 gas flow rate ratio was changed from 200 : 800 to 800 : 200, as shown in Fig. 2(f). The passivation quality increased when the doping concentration was increased from 8×10^{19} cm^{-3} to 1.8×10^{20} cm^{-3} but started to decrease rapidly with a further increase in the doping concentration from 1.8×10^{20} cm^{-3} to 4.5×10^{20} cm^{-3}. This implies that a decrease in iV_{OC} with an increase in doping concentration will be caused by in-diffusion because in-diffusion increases as the doping concentration increases, as shown Fig. 2(f). Additionally, the decrease in iV_{OC} could be due to the precipitates or clusters from the inactive P because the doping concentration at poly-Si is higher than the solubility limit, which is 4×10^{20} cm^{-3} at 950 °C.[44] The reason for the increase in iV_{OC} with an increase in doping concentration is not clearly understood in our study. However, we suggest some possibilities that a high doping concentration would increase the field effect or gettering.

(1) Field effect by doping concentration at poly-Si. According to the TSU-ESAKI tunneling current model,[45] the tunneling current is a function of the transmission coefficient (TC), which is determined by calculating the barrier height between c-Si/SiO_x and the supply function. These, in turn, are determined using the difference in carrier concentration at the interfaces of the SiO_x layer. As the doping concentration at poly-Si changes from 8×10^{19} cm^{-3} to 2×10^{20} cm^{-3}, the value of ΔE_C changes from 0.291 to 0.311 eV. This results in an increase in the electron tunneling current. Therefore, we concluded that the tunneling current changes when the doping concentration at poly-Si changes.

(2) Gettering effect by doping concentration at poly-Si. The gettering effect of the poly-Si passivating contact was studied by A. Liu.[10,11] In our research, the gettering effect was confirmed by etching poly-Si/SiO_x and the in-diffused region, and re-passivating the sample using a 10 nm-thick aluminum oxide layer. We confirmed that by increasing the doping concentration from 8×10^{19} cm^{-3} to 1.8×10^{20} cm^{-3}, the bulk quality improved as iV_{OC} after etching the poly-Si/c-Si, from 693 to 705 mV. This implies that a slight increase also caused the gettering effect, with an improvement in the bulk quality. However, further increase in doping concentration caused the drop in bulk iV_{OC} from 710 to 670 mV. This might be caused by the reappearance of gettered impurities, which is also represented by Liu *et al.*[11]

Thus, we concluded that poly-Si is required for contact because SiO_x would get destroyed without poly-Si. The poly-Si layer plays the following roles: (1) contact, (2) in-diffusion barrier, and provides (3) field effect and (4) gettering. A high-quality passivating contact can be realized using thick poly-Si to reduce in-diffusion and a high doping concentration is used to enhance the passivation quality and gettering effect.

3.2 Effect of hydrogenation

The effect of hydrogenation was investigated by comparing iV_{OC} before and after hydrogenation. In Fig. 3(a–c), delta iV_{OC} represents iV_{OC} after hydrogenation on subtracting iV_{OC} before hydrogenation. Delta iV_{OC} was higher for a lower annealing temperature, shorter time, greater thickness, and lower doping concentration. This implies the following: (1) if the annealing condition is suitable for poly-Si contact with high iV_{OC}, the effect of hydrogenation decreases, and (2) if phosphorus in-diffusion critically affects iV_{OC}, the effect of hydrogenation decreases. Thus, we conclude that in-diffusion is a critical factor that must be avoided for high passivation quality. Moreover, if in-diffusion does not have a critical effect, the annealing

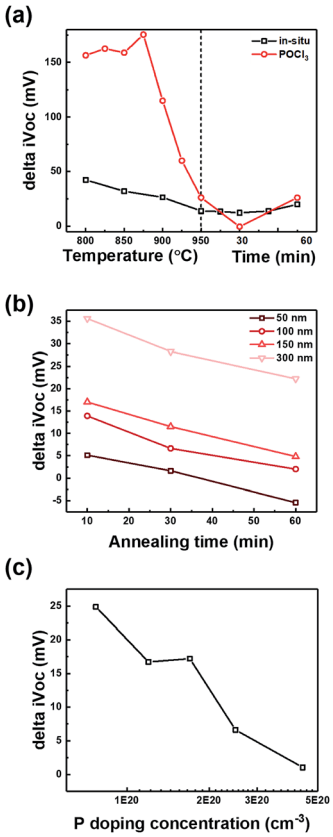

Fig. 3 Delta iV_{OC} of poly-Si passivating contacts after and before hydrogenation as a function of (a) annealing temperature, time for different doping methods, and (b) annealing time for different thicknesses, and (c) P doping concentration at poly-Si.

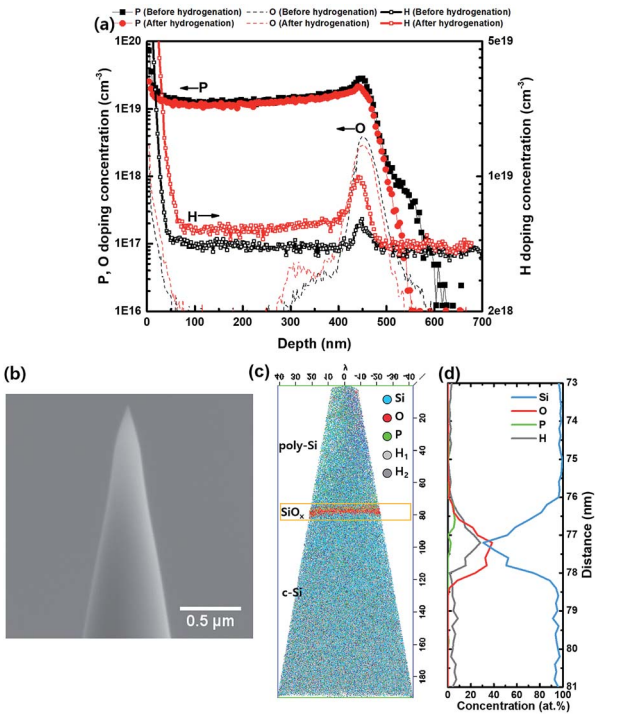

Fig. 4 (a) Doping concentration profiles of phosphorus, oxygen, and hydrogen as a function of the depth of the poly-Si passivating contact. Profiles are compared before and after hydrogenation. (b) TEM image of the poly-Si passivating contact and atom probe tomography (APT) measurement result, which shows (c) three-dimensional map of the atoms, (d) one-dimensional doping concentration graph of the interface.

condition should be controlled to maximize the passivation quality.

In Fig. 4, 2D and 3D hydrogen concentration profiles of hydrogen atoms were measured using SIMS and ATP, respectively. Fig. 4(a) demonstrates an increase in the concentration of hydrogen atoms at the SiO_x layer after hydrogenation. For the 3D profile analysis shown in Fig. 4(b–d), the peak of hydrogen concentration corresponds to that of oxygen concentration. Additionally, a slightly higher hydrogen concentration was confirmed at the surface of poly-Si/SiO_x in the 3D mapping as compared to the surface of SiO_x/c-Si. In conclusion, the result shows that the position of hydrogen atoms is correlated to the position of oxide layer.

3.2.1 iV_{OC} after etching of poly-Si. As poly-Si plays the role of (1) contact, (2) in-diffusion barrier, and provides a (3) field effect and (4) gettering, a thicker poly-Si with higher doping concentration is preferred. However, the thicker poly-Si leads to higher current loss because it has a higher infrared carrier absorption, which reduces light trapping and decreases the short-circuit current density (J_{SC}). Therefore, poly-Si should be thin to decrease the light absorption at poly-Si, which affects J_{SC}. Therefore, in this section, we etched poly-Si after hydrogenation and measured iV_{OC}. The result, which is shown in Fig. 5(a), indicates that the passivation quality is not affected owing to the etching of poly-Si. However, with further etching of poly-Si, iV_{OC} starts to decrease owing to the destruction of SiO_x. To elucidate this, TEM analysis of the poly-Si contact was performed. The TEM images, which are shown in Fig. 5(b–i), confirm that poly-Si is etched and the SiO_x layer is not affected. After etching 300 nm, the poly-Si was almost fully etched and the SiO_x layer remained, as shown in Fig. 5(e and i). This implies that (1) SiO_x is the most important passivation layer because iV_{OC} was not affected by almost completely etching the poly-Si layer, and (2) the poly-Si layer is required to protect the SiO_x layer from high-temperature annealing and hydrogenation process to enhance the passivation quality of the SiO_x layer. Therefore, the roles of poly-Si are now (1) as a contact, (2) as an in-diffusion barrier, (3) to provide the field effect and tunneling, (4) to provide gettering, and (5) as a light absorption layer, which can be etched to possess high V_{OC} and J_{SC}. The poly-Si layer is also required as a protective layer for the SiO_x layer to prevent the destruction of the SiO_x layer during process steps such as annealing, metallization, and hydrogenation.

3.2.2 Improvement in solar cell efficiency of passivating contact by etching of poly-Si. Finally, we fabricated a passivating contact silicon solar cell by etching poly-Si from 300 to 50 nm to enhance J_{SC}. First, the EQE data and reflectance graph showed that the etching of poly-Si increased the rear reflection, which thereby increased the EQE at the short and long wavelengths, as

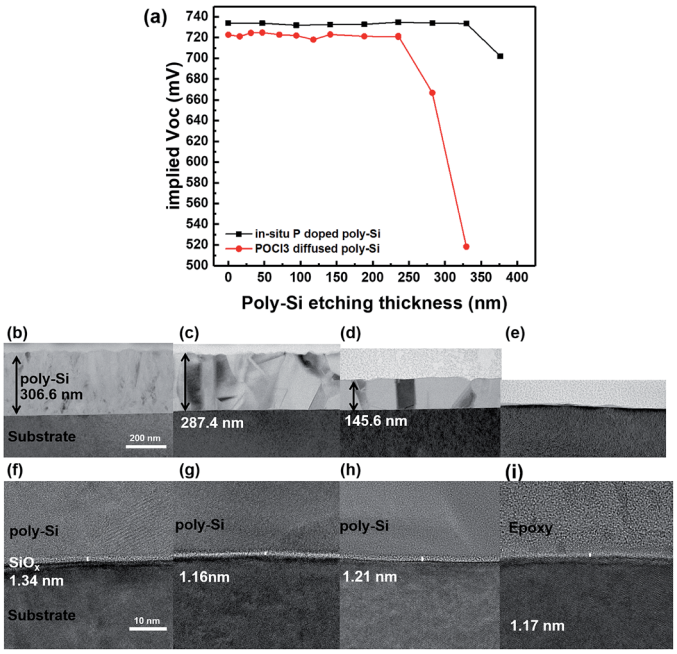

Fig. 5 (a) iV_{OC} as a function of poly-Si etching thickness and TEM images of $POCl_3$ diffused poly-Si contacts (b) before annealing, (c) after annealing at 950 °C for 30 min, and after the etching of poly-Si measuring (d) 150 nm and (e) 300 nm. (f, g, h, i) more magnified images of (b, c, d, e), respectively.

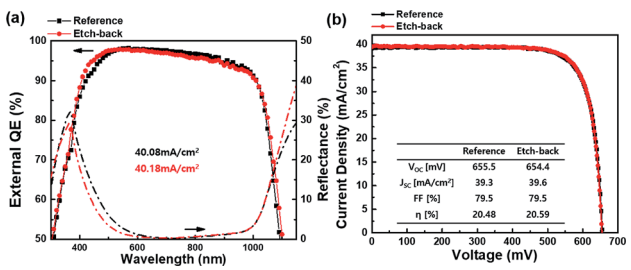

Fig. 6 (a) EQE and reflectance graph, and (b) *IV* curve.

shown in Fig. 6(a). Moreover, for the cell, J_{SC} increased from 39.3 to 39.6 mA cm^{-2} and the efficiency increased from 20.48% to 20.59% by etching poly-Si from 300 to 50 nm, with a constant fill factor and slightly decreased V_{OC}. Finally, we confirmed that the etching of poly-Si does not affect V_{OC} and the passivation quality but further enhances J_{SC} by reducing the loss caused by light absorption.

4 Summary

In this study, the roles of poly-Si were elucidated by varying the annealing temperature and time, as well as the thickness and doping concentration of poly-Si. The results indicated that poly-Si played the role of (1) contact, as the different doping concentrations of poly-Si can change the work function and cause different selectivity, (2) barrier layer for metallization and in-diffusion, as poly-Si is needed between SiO_x and metal to avoid the destruction of SiO_x layer and maintain the passivation quality, and (3) gettering, which improves the bulk quality. Moreover, by analyzing the hydrogenation concentration after hydrogenation, we confirmed that hydrogen passivation at SiO_x is important to achieve high iV_{OC}. To further improve the cell efficiency, we etched a poly-Si layer and found that the measured iV_{OC} was not affected after the etching of this layer. By compiling all results, we concluded that the efficiency of the passivating contact silicon solar cell was improved by etching poly-Si *via* facilitation of high-quality passivation and low IR carrier absorption. Finally, the solar cell exhibited increased efficiency from 20.48% to 20.59% owing to the increased J_{SC} from 39.3 to 39.6 mA cm^{-2} with a constant V_{OC} and fill factor.

Conflicts of interest

There are no conflicts to declare.

Acknowledgements

This research was supported by the New & Renewable Energy Core Technology Program of the Korea Institute of Energy Technology Evaluation and Planning (KETEP), a financial grant from the Ministry of Trade, Industry & Energy, Republic of Korea (No. 20163030014020), and the Technology Development Program to Solve Climate Changes of the National Research Foundation (NRF) funded by the Ministry of Science and ICT (NRF-2017M1A2A2087351). This work was supported by the "Human Resources Program in Energy Technology" of the Korea Institute of Energy Technology Evaluation and Planning (KETEP), with financial support from the Ministry of Trade, Industry and Energy, Republic of Korea (No. 20154030200760).

References

1 A. Richter, M. Hermle and S. W. Glunz, *IEEE J. Photovolt.*, 2013, **3**, 1184–1191.
2 U. Würfel, A. Cuevas and P. Würfel, *IEEE J. Photovolt.*, 2014, **5**, 1–9.
3 S. W. Glunz and F. Feldmann, *Sol. Energy Mater. Sol. Cells*, 2018, **185**, 260–269.
4 X. You-Peng, G. Chao, W. Tao and Z. Lang, *Acta Phys. Sin.*, 2017, **66**, 158801.
5 C. Battaglia, A. Cuevas and S. De Wolf, *Energy Environ. Sci.*, 2016, **9**, 1552–1576.
6 J. Melskens, B. W. H. van de Loo, B. Macco, L. E. Black, S. Smit and W. M. M. Kessels, *IEEE J. Photovolt.*, 2018, **8**, 373–388.
7 F. Feldmann, G. Nogay, J. Polzin, B. Steinhauser, A. Richter, A. Fell, C. Schmiga, M. Hermle and S. W. Glunz, *IEEE J. Photovolt.*, 2018, **8**, 1503–1509.
8 F. Feldmann, M. Bivour, C. Reichel, M. Hermle and S. W. Glunz, *28th European PV solar energy conference and exhibition*, 2013.
9 U. Römer, R. Peibst, T. Ohrdes, B. Lim, J. Krügener, E. Bugiel, T. Wietler and R. Brendel, *Sol. Energy Mater. Sol. Cells*, 2014, **131**, 85–91.

10 A. Liu, D. Yan, S. P. Phang, A. Cuevas and D. Macdonald, *Sol. Energy Mater. Sol. Cells*, 2018, **179**, 136–141.
11 A. Liu, D. Yan, J. Wong-Leung, L. Li, S. P. Phang, A. Cuevas and D. Macdonald, *ACS Appl. Energy Mater.*, 2018, **1**, 2275–2282.
12 D. Yan, A. Cuevas, J. Bullock, Y. Wan and C. Samundsett, *Sol. Energy Mater. Sol. Cells*, 2015, **142**, 75–82.
13 B. Nemeth, D. L. Young, M. R. Page, V. LaSalvia, S. Johnston, R. Reedy and P. Stradins, *J. Mater. Res.*, 2016, **31**, 671–681.
14 F. Feldmann, M. Bivour, C. Reichel, H. Steinkemper, M. Hermle and S. W. Glunz, *Sol. Energy Mater. Sol. Cells*, 2014, **131**, 46–50.
15 K. Masuko, M. Shigematsu, T. Hashiguchi, D. Fujishima, M. Kai, N. Yoshimura, T. Yamaguchi, Y. Ichihashi, T. Mishima, N. Matsubara, *et al.*, *IEEE J. Photovolt.*, 2014, **4**, 1433–1435.
16 K. Yoshikawa, H. Kawasaki, W. Yoshida, T. Irie, K. Konishi, K. Nakano, T. Uto, D. Adachi, M. Kanematsu, H. Uzu and K. Yamamoto, *Nat. Energy*, 2017, **2**, 17032.
17 M. A. Green, Y. Hishikawa, E. D. Dunlop, D. H. Levi, J. Hohl-Ebinger, M. Yoshita and A. W. Ho-Baillie, *Prog. Photovoltaics Res. Appl.*, 2019, **27**, 3–12.
18 M. Taguchi, A. Yano, S. Tohoda, K. Matsuyama, Y. Nakamura, T. Nishiwaki, K. Fujita and E. Maruyama, *IEEE J. Photovolt.*, 2014, **4**, 96–99.
19 K. Masuko, M. Shigematsu, T. Hashiguchi, D. Fujishima, M. Kai, N. Yoshimura, T. Yamaguchi, Y. Ichihashi, T. Mishima, N. Matsubara, *et al.*, *IEEE J. Photovolt.*, 2014, **4**, 1433–1435.
20 A. Richter, J. Benick, F. Feldmann, A. Fell, M. Hermle and S. W. Glunz, *Sol. Energy Mater. Sol. Cells*, 2017, **173**, 96–105.
21 E. Yablonovitch, T. Gmitter, R. Swanson and Y. Kwark, *Appl. Phys. Lett.*, 1985, **47**, 1211–1213.
22 A. Rohatgi, B. Rounsaville, Y.-W. Ok, A. M. Tam, F. Zimbardi, A. D. Upadhyaya, Y. Tao, K. Madani, A. Richter, J. Benick, *et al.*, *IEEE J. Photovolt.*, 2017, **7**, 1236–1243.
23 P. Brüesch, T. Stockmeier, F. Stucki and P. Buffat, *J. Appl. Phys.*, 1993, **73**, 7677–7689.
24 L. Elstner, E. Conrad, H. Eschrich, W. Füssel and H. Flietner, *Phys. Status Solidi B*, 1996, **194**, 79–90.
25 F. Haase, C. Hollemann, S. Schäfer, A. Merkle, M. Rienäcker, J. Krügener, R. Brendel and R. Peibst, *Sol. Energy Mater. Sol. Cells*, 2018, **186**, 184–193.
26 T. Wietler, D. Tetzlaff, J. Krügener, M. Rienäcker, F. Haase, Y. Larionova, R. Brendel and R. Peibst, *Appl. Phys. Lett.*, 2017, **110**, 253902.
27 G. Yang, A. Ingenito, O. Isabella and M. Zeman, *Sol. Energy Mater. Sol. Cells*, 2016, **158**, 84–90.
28 G. Yang, A. Ingenito, N. van Hameren, O. Isabella and M. Zeman, *Appl. Phys. Lett.*, 2016, **108**, 033903.
29 M. K. Stodolny, J. Anker, B. L. Geerligs, G. J. Janssen, B. W. van de Loo, J. Melskens, R. Santbergen, O. Isabella, J. Schmitz, M. Lenes, *et al.*, *Energy Procedia*, 2017, **124**, 635–642.
30 H. Park, H. Park, S. J. Park, S. Bae, H. Kim, J. W. Yang, J. Y. Hyun, C. H. Lee, S. H. Shin, Y. Kang, *et al.*, *Sol. Energy Mater. Sol. Cells*, 2019, **189**, 21–26.
31 G. Nogay, J. Stuckelberger, P. Wyss, Q. Jeangros, C. Allebé, X. Niquille, F. Debrot, M. Despeisse, F.-J. Haug, P. Löper and C. Ballif, *ACS Appl. Mater. Interfaces*, 2016, **8**, 35660–35667.
32 A. Ulyashin, R. Job, M. Scherff, M. Gao, W. Fahrner, D. Lyebyedyev, N. Roos and H.-C. Scheer, *Thin Solid Films*, 2002, **403–404**, 359–362.
33 K. v. Maydell, E. Conrad and M. Schmidt, *Prog. Photovoltaics Res. Appl.*, 2006, **14**, 289–295.
34 T. Wang, E. Iwaniczko, M. Page, D. Levi, Y. Yan, H. Branz and Q. Wang, *Thin Solid Films*, 2006, **501**, 284–287.
35 M. Jeon, S. Yoshiba and K. Kamisako, *Curr. Appl Phys.*, 2010, **10**, S237–S240.
36 Y. Lee, S. Han, S. Kim, S. Md Iftiquar, Y.-J. Lee, J. Yoo, A. Dao and J. Yi, *J. Photonics Energy*, 2014, **4**, 043094.
37 A. Richter, J. Benick, F. Feldmann, A. Fell, M. Hermle and S. W. Glunz, *Sol. Energy Mater. Sol. Cells*, 2017, **173**, 96–105.
38 S. Choi, K. Hong Min, M. Sang Jeong, J. In Lee, M. G. Kang, H.-E. Song, Y. Kang, H.-S. Lee, D. Kim and K.-H. Kim, *Sci. Rep.*, 2017, **7**, 12853.
39 H. T. Nguyen, A. Liu, D. Yan, H. Guthrey, T. N. Truong, M. Tebyetekerwa, Z. Li, Z. Li, M. M. Al-Jassim, A. Cuevas and D. Macdonald, *ACS Appl. Energy Mater.*, 2018, **1**, 6619–6625.
40 A. Moldovan, F. Feldmann, M. Zimmer, J. Rentsch, J. Benick and M. Hermle, *Sol. Energy Mater. Sol. Cells*, 2015, **142**, 123–127.
41 H. Steinkemper, F. Feldmann, M. Bivour and M. Hermle, *IEEE J. Photovolt.*, 2015, **5**, 1348–1356.
42 R. A. Sinton and A. Cuevas, *Appl. Phys. Lett.*, 1996, **69**, 2510–2512.
43 H. Kim, S. Bae, K.-s. Ji, S. M. Kim, J. W. Yang, C. H. Lee, K. D. Lee, S. Kim, Y. Kang, H.-S. Lee, *et al.*, *Appl. Surf. Sci.*, 2017, **409**, 140–148.
44 H. Wagner, A. Dastgheib-Shirazi, B. Min, A. E. Morishige, M. Steyer, G. Hahn, C. del Cañizo, T. Buonassisi and P. P. Altermatt, *J. Appl. Phys.*, 2016, **119**, 185704.
45 R. Tsu and L. Esaki, *Appl. Phys. Lett.*, 1973, **22**, 562–564.